CHARACTERIZATION AND DETERMINATION OF MECHANICAL PROPERTIES OF YBCO SUPERCONDUCTING THIN FILMS WITH MANGANESE USING THE TFA-MOD METHOD

KARAKTERIZACIJA IN DOLOČITEV MEHANSKIH LASTNOSTI SUPERPREVODNE TANKE PLASTI YBCO Z MANGANOM PO METODI TFA-MOD

Osman Culha[1], Isil Birlik[2], Mustafa Toparli[2], Erdal Celik[2], Sebastian Engel[3], Bernhard Holzapfel[3]

[1]Celal Bayar University, Department of Materials Engineering, Muradiye Campus, Manisa, Turkey
[2]Dokuz Eylul University, Department of Metallurgy and Materials Engineering, Tinaztepe Campus, Buca, Izmir, Turkey
[3]Leibniz-Institut für Festkörper- und Werkstoffforschung (IFW), Solid-State and Materials Research, Helmholtzstraße 20, 01069 Dresden, Germany
isil.kayatekin@deu.edu.tr

The aim of this study is to determine the microstructure, superconducting and mechanical properties of $YBa_2Cu_3O_{6.56}$ (YBCO) and YBCO thin films with a manganese (Mn) addition. All the YBCO superconducting films (undoped and Mn-doped) were dip-coated onto (001) $SrTiO_3$ (STO) single-crystal substrates with a metalorganic deposition using the trifluoroacetate (TFA-MOD) technique. The phase analysis, microstructure, surface morphologies and critical temperature (T_c) of the superconducting thin films were determined with an X-ray diffractometer (XRD), a scanning electron microscope (SEM), an atomic force microscope (AFM) and an inductive T_c measurement system. Since the main issue of this study is to determine the mechanical-property variations of the superconducting thin films with/without a Mn addition, the adhesion strength of these films on a STO substrate was tested with a Shimadzu scratch tester. Depending on the Mn addition, the critical forces of pure films increase from 56.23 mN, 58.63 mN and 60.11 mN for pure YBCO, YBCO with 0.05 g and 0.10 g of Mn. Furthermore, Young's modulus and the hardness of the undoped and Mn-doped YBCO thin films were measured with a CSM Berkovich nanoindenter using the load-unload sensing analysis under a 0.3 mN applied load.

Keywords: superconducting films, sol-gel synthesis, mechanical properties, nanoindentation

Namen te študije je določiti mikrostrukturo, superprevodne in mehanske lastnosti $YBa_2Cu_3O_{6.56}$ (YBCO) in tanke plasti YBCO z dodatkom mangana (Mn). Vse superprevodne plasti YBCO (nedopirane in dopirane z Mn) so bile nanesene na monokristalni substrat (001) $SrTiO_3$ (STO) s kovinoorganskim nanosom s trifluoroacetatno tehniko (TFA-MOD). Fazna analiza, mikrostruktura, morfologija površine in kritična temperatura (T_c) superprevodne tanke plasti so bile določene z rentgenskim difraktometrom (XRD), vrstičnim elektronskim mikroskopom (SEM), mikroskopom na atomsko silo (AFM) in induktivnim merilnim sistemom za T_c. Ker je bila glavna naloga te študije določanje spreminjanja mehanskih lastnosti YBCO z dodatkom Mn in brez njega, je bila preizkušena adhezivnost te plasti na STO-podlago s Shimadzu preizkuševalnikom za razenje. Odvisno od dodatka Mn kritična sila v čisti plasti narašča od 56,23 mN, 58,63 mN in 60,11 mN za čisti YBCO, YBCO z 0,05 g in 0,10 g Mn. Poleg tega sta bila izmerjena tudi Youngov modul in trdota nedopirane in z Mn dopirane tanke plasti YBCO z nanomerilnikom trdote CSM Berkovich z analizo zaznavanja obremenjeno – neobremenjeno pri uporabljeni obremenitvi 0,3 mN.

Ključne besede: superprevodna plast, sol-gel sinteza, mehanske lastnosti, nanopreizkušanje trdote

1 INTRODUCTION

After the discovery of high-T_c superconductors (HTS), their various applications have been tested in various areas. These materials are supposed to increase the performance of devices such as magnetic resonance imaging (MRI) in medicine, energy-storage systems in a transformer, magnetic separators, levitation, nuclear magnetic resonance (NMR), generators, engines, cables, superconducting wires and tapes, accelerators, electro-magnets, electronic transistors and bolometers.[1,2]

HTS thin films with a sharp resistive transition, high critical current density J_c and low flux noise offer the potential for such applications.[3] Extensive studies are currently being carried out worldwide on $YBa_2Cu_3O_{6.56}$ (YBCO) films grown on different single-crystal and metal-based substrates[4]. Many YBCO thin films have

been developed using different deposition processes. Most of them use high vacuum techniques such as pulse laser deposition (PLD) and magnetron sputtering that can create high critical current densities on YBCO thin films. Nevertheless, they require significant start-up costs for long-length coated-conductor production[5]. On the other hand, thin films prepared with non-vacuum techniques like metal-organic decomposition using triflouroacetic acid (TFA-MOD) which is a sol-gel-related method, show similar superconducting properties and are relatively simple and inexpensive[6]. High-quality YBCO films with high J_c can be fabricated in a TFA-MOD process[7]. Finding the optimum process parameters for a coating solution can be challenging, but once the coating solution is found, it is very easy to obtain high J_c YBCO superconductors with supreme reproducibility. Although the TFA-MOD process using

metal acetates as the starting materials is more cost effective than vacuum processes, the highly purified metal acetates are expensive and thus it is desirable to find a more economic route. Recently, several attempts to use oxide powders, such as the commercially available YBCO powder, as the starting materials have been reported and they have shown high J_c for the YBCO films compared to the other methods.[8]

In this paper we present a new approach by combining the superior properties of a solvent, especially 2,4-pentanedionate, and a commercially available YBCO powder with TFA, acetone and propionic acid as the preliminary study. Therefore, YBCO superconducting films were produced with $BaMnO_3$ from the solutions prepared with the cheap and commercially available YBCO powders and Mn 2,4-pentanedionate, TFA propionic acid and acetone. In practical applications, the importance of the mechanical properties of YBCO-based films cannot be ignored. Superconducting films with poor mechanical properties are useless, even if they possess good transport and flux-pinning properties. Since an addition of particles as pinning centers results in important changes on the microstructure of thin films, their effect on micromechanical properties such as Young's modulus, hardness and adhesion strength also have to be investigated with respect to the particles type and quantity.

2 THEORETICAL BACKGROUND FOR MECHANICAL PROPERTIES

The scratch test is used to measure the interfacial adhesion for a range of different coatings.[9–19] During the test, a diamond indenter is drawn over the surface of a sample tested under a normal force, which is increased either stepwise or continuously until the critical normal force is reached, at which a well defined coating failure occurs.[9] Then, force is taken as a measurement of the adhesion between the coating and the substrate. The onset of a coating failure can be monitored with optical microscopy, acoustic emission (AE) and friction-force measurements[10]. It has been suggested that the coating adhesive failure is directly associated with a sudden increase in the friction force.[11,12] It is generally accepted that the scratch test is suitable for the coatings of a thickness ranging from 0.1 μm to 20 μm and this covers a large number of engineering applications.[13]

The adhesion strength (F) of the films was calculated by using equation (1) for the average value of three measurements. The scratch was examined with an optical microscope and the critical load, at which the coating was removed, was determined. The adhesion strength, F (in MPa), was calculated by using equation (1):[20]

$$F = \frac{H}{\left[(\pi R^2 H - W_c) / W_c \right]^{1/2}} \quad (1)$$

where H is the Brinell hardness value (kg mm^{-2}) of the $SrTiO_3$ (STO) substrate and R is the radius of the stylus (μm) and W_c is the critical force.

On the other hand, indentation tests are used to determine elasto-plastic properties such as Young's modulus, yield strength and the strain-hardening exponent[21] of thin films. Young's modulus may be inferred from the unloading indentation load-depth curve and the yield strength from the maximum indentation load. In addition, a method to extract the flow stress and the strain-hardening exponent using indentation data has been researched.[22–27] The indentation hardness of materials is measured in several ways by forcing an indenter having a specific geometry (ball, cone, and pyramid) into a specimen's surface.[28] The conventional microhardness value can be determined with an optical measurement of the residual impression left behind upon a load release. The development of depth-sensing indentation equipment has allowed an easy and reliable determination of two of the most commonly measured mechanical properties of materials: the hardness and Young's modulus.[26,29]

Two mechanical properties, namely, elastic modulus (E) and microhardness (H) can be obtained from the load and penetration-depth data. A typical load-penetration-depth curve can be investigated using a related reference.[30] During an indenter loading, the test material is subjected to both elastic and plastic deformations. One of the challenges in studying mechanical properties of thin films is that the traditional methods used to evaluate mechanical properties of bulk materials are not applicable for thin films and so far there is no standard test method for the evaluation of mechanical properties of thin films.[31] New methods, such as depth-sensing nanoindentation, microbridge test, uniaxial tensile test and ultrasonic method are being developed[32–35] for the measurement of mechanical properties of thin films. Among these methods, the depth-sensing nanoindentation technique provides a continuous record of the variation of indentation load with the penetration depth into a specimen and this technique has been an area of considerable attention in recent years due to its high resolution at a low load scale. Currently, the nanoindentation technique is being applied to determine hardness and Young's modulus, while limited studies are available to develop an effective method to obtain the plastic properties of thin films with a nanoindentation technique. For example, Nix[34] has utilized a nanoindentation technique to study the strength properties of thin films. Giannakopoulos and Suresh[32] have developed a step-by-step method to obtain the mechanical properties of materials from the nanoindentation experimental data. The indentation response of a thin film on a substrate is a complex function of the elastic and plastic properties of both the film and the substrate and it is essential to understand how the intrinsic mechanical properties of a film can be determined from the overall mechanical response of a film/substrate system. As the values of

154

elastic modulus and hardness, determined from indentations, should not depend on the value of h (indentation depth) and, therefore, on the value of the maximum load, the indentation depth should not exceed 10–20 % of the coating thickness, otherwise the results will be affected by the properties of the substrate.[21–30]

3 EXPERIMENTAL PROCEDURE

3.1 Preparation of the solutions

Y-Ba-Cu-O based solution was prepared from a commercial $YBa_2Cu_3O_{6.56}$ powder (yttrium-barium-copper oxide) with propionic acid, trifluoroacetic acid (TFA), acetone and 2,4-pentanedionate under atmospheric conditions at room temperature. The 8.3045 g YBCO powder was weighted out in order to prepare a 0.25 M and 50 ml solution. After 10 ml of propionic acid was added to the YBCO powder, the mixture was being dissolved in 25 ml of TFA at 45 °C for 60 min using an ultrasonic mixer (Sonorex digital 10P). The solvents were being removed at 100 °C for 60 min with a hot plate to yield a blue-sticky-glassy residue with a high viscosity. The solution of the film was made by dissolving the residue with up to 50 ml of TFA. The solvents were being evaporated from the solution again at 60 °C for 60 min until a highly viscous solution of a transparent-blue colour was obtained. After adding up to 50 ml of acetone into the solution, 15 ml of propionic acid and 5 ml of TFA were incorporated into the obtained viscous solution, and then a standard transparent solution was prepared. Finally, Mn alkoxide was separately added into 5 ml of the transparent solution with a low content of 2,4-pentanedionate as presented by the flow chart in **Figure 1**.

3.2 Coating process

Initially, (100) STO single-crystal substrates with the dimensions of 10 mm × 10 mm × 0.75 mm were rinsed in acetone using a standard ultrasonic cleaner. After that, the solutions were deposited on the substrates during a dip-coating process with a withdrawal speed of 0.3 cm/s in a vacuum atmosphere. The dip coating involves a formation of a film through a liquid-entrainment process that may be either batch or continuous in nature. The general steps include an immersion of the substrate into the dip-coating solution, a start-up, during which a withdrawal of the substrate from the solution begins, a film deposition, a solvent evaporation, and a continued drainage as the substrate is completely removed from the liquid bath. The film thickness formed in dip coating is mainly governed by the viscous drag, gravitational forces, and the surface tension.

The deposited gel films were converted to an epitaxial pure YBCO and a YBCO film with $BaMnO_3$ nanoparticles through a combination of the calcining and heat-treatment procedures. The gel film was dried from
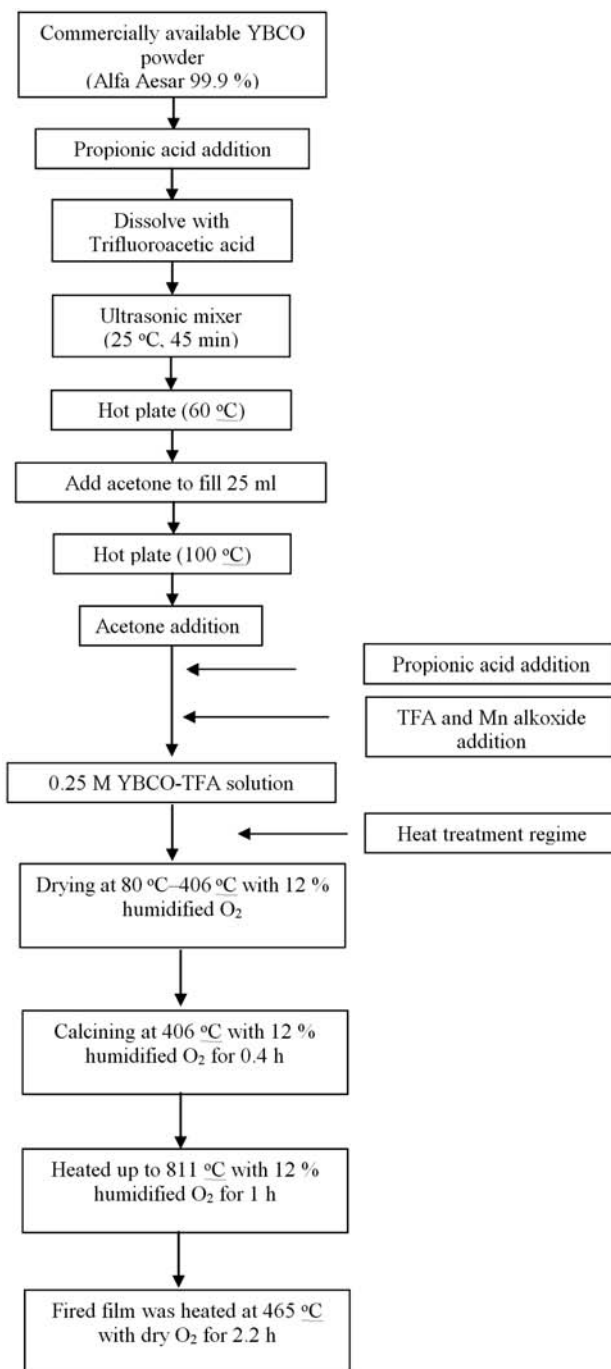

Figure 1: Flow chart of the TFA-MOD technique
Slika 1: Potek postopka TFA-MOD

80 °C to 406 °C in 12 % humidified oxygen. After the calcining was performed at 406 °C for 0.4 h in 12 % humidified nitrogen, the film was being heated up to 811 °C for 1 h in 12 % humidified nitrogen and the fired film was consequently heat treated at 465 °C for 2.2 h in a dry oxygen atmosphere. In order to obtain highly textured thin films on the STO substrate, the oxygen content was 500 ml O_2 during the heat-treatment process at 465 °C for 2.2 h as expressed in **Figure 1**.

3.3 Characterization process

The structural development of the produced thin films was investigated using X-ray diffraction (XRD-Rigaku D/MAX-2200/PC) patterns, recorded using the Co Kα irradiation (wavelength, λ = 0.178897 nm) and the scanning range was between 2θ = 10° and 90°. The surface topographies and additional particle effects on the microstructure of the films were examined with a high resolution SEM (JEOL JSM 6060). The surface morphologies of the films were measured with an atomic force microscope (AFM). The resistivity-temperature behaviors of the superconductive thin films were determined and the critical temperatures, T_c, were obtained depending on the additional particle content.

3.4 Mechanical properties of the films

The load on a Rockwell C diamond with a tip radius of the stylus (R) of 15 μm was linearly increased from 0 mN to 98 mN at the loading speed of 1 mN/s for the scratch test. In addition, the scratch speed of the diamond tip was 2 μm/s. The testing temperature and humidity percentage were 20.3 °C and 50 %, respectively. The scratch was examined with an optical microscope and the critical force (W_c) value, at which the coating removed from the substrate was determined three times for each sample. The hardness and Young's modulus of the produced thin films were measured under 0.3 mN of the applied peak load three times with the CSM Berkovich nanoindentation tester (the loading-unloading test mode) to determine additional particle effects on mechanical properties.
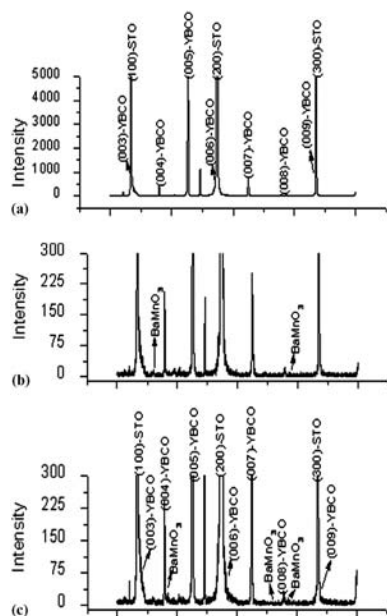
4 RESULTS AND DISCUSSION

4.1 Characterization of the films

Figure 2 (**a–c**) shows the XRD patterns of pure YBCO, YBCO with 0.05 g and 0.10 g Mn on the STO single-crystal substrate obtained with the TFA-MOD method. XRD patterns showed that the pure YBCO film has (001) major diffraction peaks corresponding to the
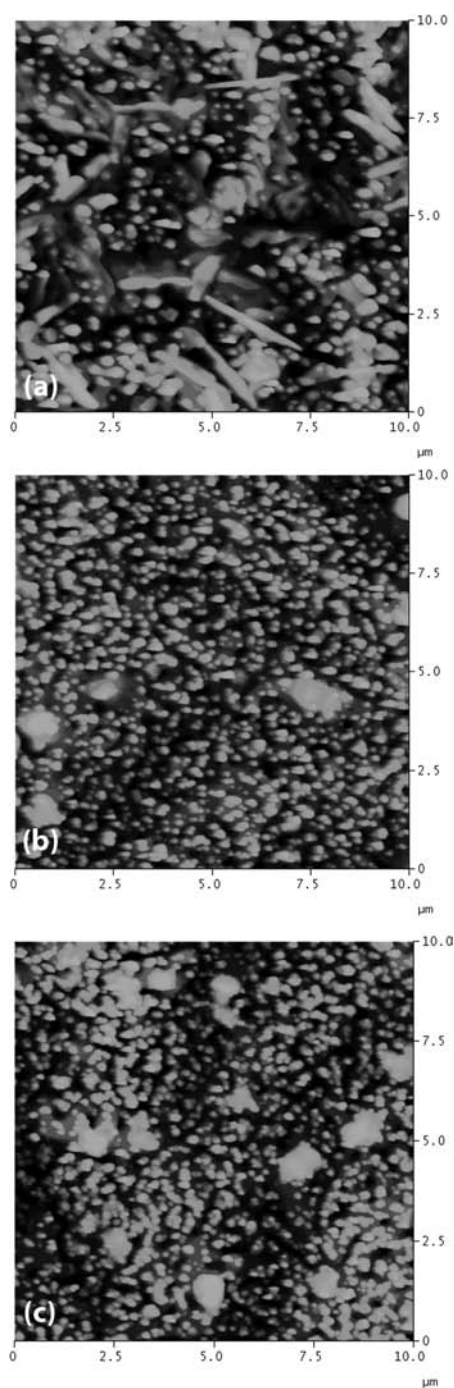

Figure 3: AFM study of YBCO thin films with: a) 0 g, b) 0.05 g and c) 0.10 g BaMnO$_3$ nanoparticles
Slika 3: AFM-študija YBCO tanke plasti z: a) 0 g, b) 0,05 g in c) 0,10 g BaMnO$_3$ nanodelci

Figure 2: XRD patterns of: a) pure YBCO, b) YBCO with 0.05 g and c) 0.10 g BaMnO$_3$ nanoparticles
Slika 2: Rentgenski praškovni posnetki (XRD): a) čisti YBCO, b) YBCO z 0,05 g in c) 0,10 g BaMnO$_3$ nanodelci

(00l) parallel plane. It is worth mentioning that YBCO films with a high intensity were grown on the STO substrate using the TFA-MOD method. In addition, no second phases such as $Y_2Cu_2O_5$, BaF_2 and CuO were found in the case, where only a pure YBCO phase was formed. Apart from that, $BaMnO_3$ perovskite peaks with a low intensity were determined on account of the Mn-doping effect. However, XRD peaks from the $BaMnO_3$ perovskite second phase were hardly detected even for the film that was prepared using a precursor solution containing a 0.10 g Mn dopant.

The effects of $BaMnO_3$ nanoparticles on the microstructure of YBCO thin films were identified in **Figure 3**. According to the AFM results, all the films show typical CuO_x precipitatates with 100–200 nm diameters, which are regularly found on the surface of TFA-MOD samples. When the Mn content increased from 0 g to 0.10 g, the surface-roughness values of pure YBCO thin films and the YBCO thin films with $BaMnO_3$ nanoparticles changed from 21 nm to 33 nm depending on the Mn doping content. Nevertheless, a clear change in the YBCO surface was observed.

Figures 4, 5 and **6** show SEM micrographs of pure YBCO and the YBCO films with $BaMnO_3$ nanoparticles. Figure 4 shows surface topographies of the pure YBCO film with the a-axis which decrease the superconducting properties. These films were produced using the standard YBCO transparent solution. However, the decreasing superconducting properties with the a-axis were eliminated using the Mn doping in the standard YBCO precursor solution as clearly depicted in **Figures 5** and **6**. SEM micrographs indicate that structural defects can be reacted as nanodots or nanoparticles (due to the Mn addition) along the *c*-axis of the YBCO film. These properties result in an enhanced pinning over the pure YBCO film. Since Mn reacts with Ba and a $BaMnO_3$ perovskite structure forms in the YBCO film during the
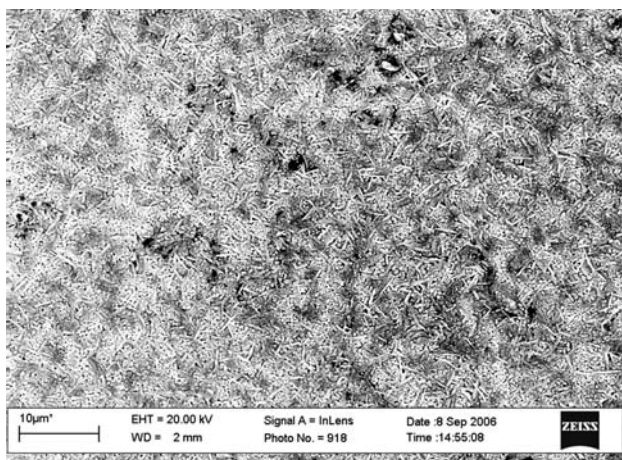

Figure 5: Surface morphology of an YBCO film with $BaMnO_3$ nanoparticles produced using the YBCO transparent solution with 0.05 g Mn doping
Slika 5: Morfologija površine YBCO tanke plasti z $BaMnO_3$ nanodelci, izdelane s prozorno raztopino YBCO, dopirano z 0,05 g Mn
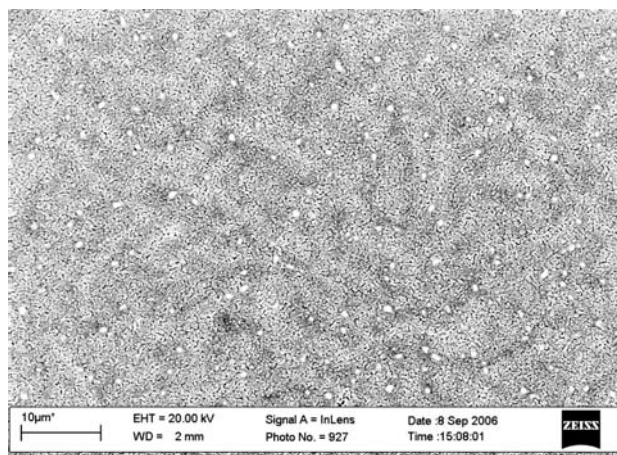
Figure 6: Surface morphology of an YBCO film with $BaMnO_3$ nanoparticles produced using the YBCO transparent solution with 0.10 g Mn doping
Slika 6: Morfologija površine YBCO tanke plasti z $BaMnO_3$ nanodelci, izdelane s prozorno raztopino YBCO, dopirano z 0,10 g Mn

heat-treatment process, the microstructures of superconducting thin films were changed as expected.

The dependences of the inductively measured critical transition temperature (T_c) and transition width (ΔT_c) on the amount of $BaMnO_3$ in the structure are shown in **Figure 7**. It can be seen that there is sharp decrease in the resistivity near 90 K where the critical-temperature value of pure YBCO is 90.4 K. When the quantity of additional particles increases from 0.05 g to 0.10 g, the critical temperature changes from 90.2 K to 90 K. These additional particles do not affect the critical temperature and only behave as impurities or second phases for the flux-pinning properties.

Figure 4: Surface morphology of a pure YBCO film with the a-axis produced using the standard YBCO transparent solution
Slika 4: Morfologija površine čiste plasti YBCO z a-osjo, izdelane s standardno prozorno raztopino YBCO
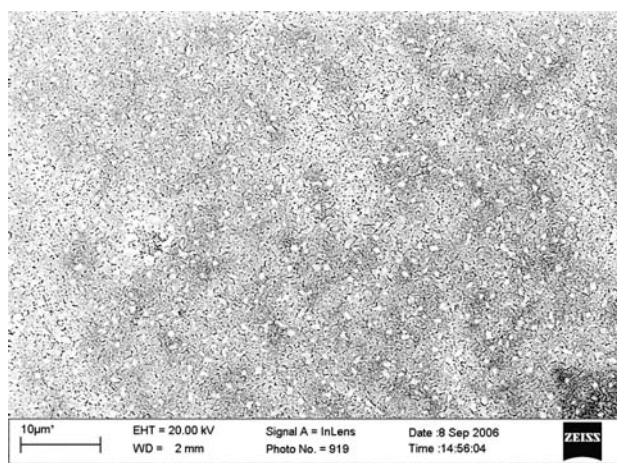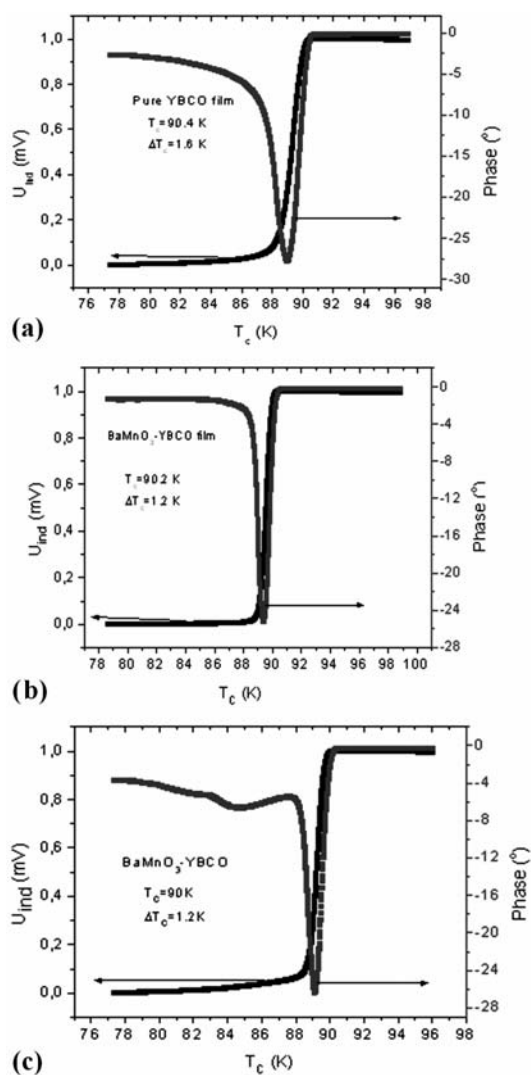
Figure 7: Critical-temperature values of YBCO thin films with: a) 0 g, b) 0.05 g and c) 0.10 g BaMnO$_3$ nanoparticles

Slika 7: Vrednosti kritične temperature YBCO tanke plasti z: a) 0 g, b) 0,05 g in c) 0,10 g BaMnO$_3$ nanodelci

4.2 Determination of mechanical properties

The analysis of the scratch test gives critical-force values of the produced thin films. These critical-force values correspond to the first peak in the cartridge output percentage – the test force graphical curve obtained from the scratch-test machine. The bond strengths, critical-force and Brinell-hardness values of pure YBCO and YBCO with BaMnO$_3$ nanoparticles are presented in **Table 1**. The hardness value of the substrate was converted to Brinell hardness (*H*) with the Standard Hardness Conversion Tables for Metal and the adhesion strength (*F*) of the coatings was calculated as a MPa unit using equation (1).[20] It is clearly seen from **Table 1** that pure YBCO, the YBCO thin films with 0.05 g and 0.1 g of BaMnO$_3$ nanoparticles have the critical forces of 56.23 mN, 58.63 mN and 60.11 mN, respectively.

Therefore, the calculated adhesion strength of the films increases from 160 MPa to 173 MPa depending on the BaMnO$_3$ formation in the microstructure.

As expected, the mechanical strength against the internal forces caused by the flux pinning rather than the magnitude of the critical current density, may become the factor limiting the performance of HTS thin films for high-current density applications. For the bulk pure YBCO material, this problem has been already discussed in [36]. In this study, an increasing J_c and an improvement in the flux-pinning properties of the YBCO films with the BaMeO$_3$ perovskite nanoparticles (Me : Mn), as the pinning centers, on SrTiO$_3$ (STO) are aimed at with the trifluoroacetic acid-metal organic deposition (TFA-MOD). Since the general purpose is to determine the mechanical properties such as Young's modulus and the hardness of a pure YBCO thin film and the YBCO thin films with a Mn addition (Mn reacts as BaMnO$_3$), an instrumented nanoindentation test was applied to both samples. This time, the importance of the applied load and the indentation size is apparent. As presented in **Table 2**, the ratios of the indentation depths and the film thicknesses are applicable for an instrumented indentation with an applied load of 300 μN. A smoothing procedure was applied to all of the instrumented indentation results of the samples. Another parameter, which can affect the indentation test, is the surface roughness. It has a very active role in an indentation experiment at the nanoscale. If the surface roughness is larger than the maximum indentation depth, the curve has very scattered data characteristic for the loading and unloading parts.

Table 1: Brinell hardness, critical force and bond strengths of YBCO and YBCO with Mn
Tabela1: Trdota po Brinellu, kritična sila in trdnost vezave YBCO in YBCO z Mn

Sub-strate	Brinell hardness substrate (HB)	Indenter radius (μm)	Material	Average critical force (mN)	Adhesion strength (MPa)
STO	143	15	Pure YBCO	56 ± 1.2	160 ± 1.1
			YBCO with 0.05 g Mn	59 ± 1.8	168 ± 1.7
			YBCO with 0.1 g Mn	60 ± 1.6	173 ± 1.5

Table 2: Maximum depth, residual depth and film thickness of pure YBCO and YBCO with additional particles
Tabela 2: Maksimalna globina, preostala globina in debelina plasti čistega YBCO in YBCO z dodatnimi delci

Material	Force (μN)	Maximum depth (nm)	Residual depth (nm)	Film thickness (nm)
YBCO	300	40.24 ± 6.4	30.12 ± 7.8	292 ± 9
YBCO with 0.05 g Mn	300	42.32 ± 9.4	32.11 ± 8.7	297 ± 5
YBCO with 0.10 g Mn	300	42.45 ± 5.9	33.53 ± 4.4	294 ± 6

The YBCO-based thin film has suitable properties for ceramic materials, such as hardness and stiffness, together with the tendency to fracture. However, the references about the mechanical properties of this material, particularly the yield strength and the stress-strain curve, are scarce. The mechanical properties (hardness, Young's modulus and fracture toughness) of the YBCO samples have been examined with the techniques such as ultrasound[37], X-ray diffraction[38] and nanoindentation[39]. The reported values of Young's modulus for Y-123 are within the range of $E = 40–200$ GPa. This large scatter may be due to the residual porosity and a poor contact between the grains[40]. Other authors,[41] also using nanoindentation and applying the loads between 30 mN and 100 mN, reported the values of $E = 171–181$ GPa for the YBCO samples textured with the Bridgman technique, which is in agreement with Johansen. The nanohardness values in the range of 7.8–8.0 GPa at the maximum loads of 30 mN were recently reported in several researches for the bulk, single-crystal YBCO.[38–41] Roa et al. (2007) found a hardness value of (8.9 ± 0.1) GPa obtained with a nano-indentation on the YBCO samples textured with the Bridgman technique.

After obtaining the loading-unloading (load-displacement) curves, force-time and depth-time graphs for pure YBCO and the YBCO films with 0.05 g and 0.1 g Mn (reacting as BaMnO$_3$) under a applied peak load of 300 μN, some characteristic indentation parameters were listed in **Tables 2** and **3**. According to the indentation results in **Table 2**, the maximum and residual depths of the YBCO-based thin films under the same indentation loads were increased from (40.24 ± 6.4) nm to (42.45 ± 5.9) nm and from (30.12 ± 7.8) nm to (33.53 ± 4.4) nm, respectively. Furthermore, as represented in **Table 3**, the elastic modulus and indentation hardness of the YBCO-based thin films were decreased from (88.54 ± 3.1) GPa to (79.11 ± 1.9) GPa and from (12.51 ± 5.1) GPa to (5.75 ± 1.1) GPa under a load of 300 μN. Although the indentation load was fixed at 300 μN, the indentation hardness was decreased as if the indentation size affected the mechanical properties. Since the hardness is accepted as an inherent material property, it should not vary with the indentation load and size but may change with different phase formations. The indentation hardness was decreased with the formation of the BaMnO$_3$ content in the YBCO thin-film structure. According to this explanation, it can be concluded that the pure YBCO thin film is harder and more brittle than the BaMnO$_3$ additional ones. As listed in **Table 3**, the indentation hardness of the YBCO-based thin films decreased with an increased Mn content in the structure. The elastic-modulus variation of the YBCO-based thin films is also shown in **Table 3**. Although the hardness was very sensitive to the maximum indentation depth and the thickness/indentation-depth ratio of the samples and it changed from 12.51 GPa to 5.75 GPa, the elastic

modulus of the YBCO-based thin films did not show a sharp decrease. However, as listed in **Table 3**, the elastic modulus of pure YBCO, YBCO with 0.05 g Mn, and YBCO with 0.10 g Mn was calculated to be 88.54 GPa, 83.41 GPa, and 79.11 GPa, respectively. After considering the hardness and elastic modulus of the YBCO-based thin films with AFM, SEM and the critical temperature value, T_c, it was found that the second phase of BaMnO$_3$ did not continuously improve the mechanical and superconducting properties. When the Mn content increased from 0 g to 0.15 g, the BaMnO$_3$ phases occurred and made the structure more ductile than the pure one. According to the T_c measurement, a sharp decrease in T_c could be considered and the ΔT_c values of the YBCO-based films were very small up to the addition of 0.15 g Mn. In this case ΔT_c was 4.2 K for the YBCO thin film with a 0.15 g Mn addition (BaMnO$_3$) and a sharp decrease in the resistivity could not be seen easily as presented **Figure 7**.

Table 3: Indentation-experiment results for pure YBCO and YBCO with additional particles
Tabela 3: Preizkus trdote čistega YBCO in YBCO z dodanimi delci

Material	Force (μN)	Hardness (HV)	Indentation hardness (GPa)	Young's modulus (GPa)
YBCO	300	695 ± 28	12.51 ± 4.8	88.54 ± 3.1
YBCO with 0.05 g Mn	300	525 ± 16	8.21 ± 1.2	83.41 ± 1.8
YBCO with 0.10 g Mn	300	495 ± 21	5.75 ± 1.1	79.11 ± 1.9

5 CONCLUSION

In this study, YBCO films with/without the Mn solutions were prepared by dissolving commercially available YBCO powders in propionic acid, trifluoro-acetic acid (TFA) and acetone. The prepared solutions were dip coated on the STO single-crystal substrates. The following microstructural and mechanical results were obtained:

- XRD patterns show that the produced YBCO films have (001) and parallel plane reflections for pure YBCO and the YBCO with the BaMnO$_3$ thin film.
- According to the AFM study, topographic properties and the roughness of thin films were increased with an increase in the amount of nanoparticles (acting as a pinning center) in the film structure.
- SEM micrographs indicate that the structural defects consisted of the nanodots or nanoparticles of BaMnO$_3$ along the c-axis of the YBCO film. These properties resulted in an enhanced pinning over the pure YBCO film.
- It can be seen from the T_c analysis that there is a sharp decrease in the resistivity near 90 K.
- Critical force values of pure YBCO and of the YBCO-based thin films with 0.05 g and 0.1 g BaMnO$_3$ were found to be (56.23, 58.63 and 60.11)

mN, respectively. The calculated adhesion strength of the films increased from 160 MPa to 173 MPa depending on the BaMnO$_3$ addition.

- The calculated Young's modulus of YBCO thin films decreased with the BaMnO$_3$ formation. The same effects can be seen in the hardness variation of pure YBCO and the YBCO thin films with the BaMnO$_3$ nanoparticles.

6 REFERENCES

[1] N. Hari Babu, K. Iida, D. A. Cardwell, Enhanced magnetic flux pinning in nanocomposite Y-Ba-Cu-O superconductors, Physica C, 445–448 (**2006**), 353–356

[2] Y. Yoshida, K. Matsumoto, M. Miura, Y. Ichino, Y. Takai, A. Ichinose, M. Mukaida, S. Horii, Controlled nanoparticulate flux pinning structures in RE$_{1+x}$Ba$_{2-x}$Cu$_3$O$_y$ films, Physica C, 445–448 (**2006**), 637–642

[3] B. Lakew, J. C. Brasunas, S. Aslam, D. E. Pugel, High T_c, transition-edge superconducting (TES) bolometer on a monolithic sapphire membrane-construction and performance, Sensor. Actuat. A-Phys., 114 (**2004**), 36–40

[4] B. Dwir, L. Pavesi, J. H. James, B. Keilelt, D. Pavuna, F. K. Reinhart, A simple high temperature superconducting thin film optical bolometer, Supercond. Sci. Technol., 2 (**1989**), 314–316

[5] Y. A. Jee, M. Li, B. Ma, V. A. Maroni, B. L. Fisher, U. Balachandran, Comparison of texture development and superconducting properties of YBCO thin films prepared by TFA and PLD processes, Physica C, 356 (**2001**), 297–303

[6] Y. Yamada, S. Kim, T. Araki, Y. Takahashi, T. Yuasa, H. Kurosaki, Critical current density and related microstructures of TFA-MOD YBCO coated conductors, Physica C, 357 (**2001**), 1007–1010

[7] X. M. Cui, B. W. Tao, J. Xiong, X. Z. Liu, J. Zhu, Y. R. Li, Effect of annealing time on the structure and properties of YBCO films by the TFA–MOD method, Physica C, 432 (**2005**), 147–152

[8] S. Y. Lee, S. A. Song, B. J. Kim, J. A. Park, H. J. Kim, G. W. Hong, Effect of precursor composition on J_c enhancement of YBCO film prepared by TFA-MOD method, Physica C, 445–448 (**2006**), 578–581

[9] J. Lia, W. Beres, Three-dimensional finite element modelling of the scratch test for a TiN coated titanium alloy substrate, Wear, 260 (**2006**), 1232–1242

[10] P. Hedenqvist, S. Hogmark, Experiences from scratch testing of tribological PVD coatings, Tribol. Int., 30 (**1997**), 507–516

[11] J. Valli, U. Mäkelä, Applications of the scratch test method for coating adhesion assessment, Wear, 115 (**1987**), 215–221

[12] J. Sekler, P. A. Steinmann, H. E. Hintermann, The scratch test: different critical load determination techniques, Surf. Coat. Technol., 36 (**1988**), 519–529

[13] K. Holmbert, A. Matthewst, H. Ronkainen, Coatings tribology-contact mechanisms and surface design, Tribol. Int., 31 (**1998**), 107–120

[14] K. Holmbert, The basic material parameters that control friction and wear of coated surfaces under sliding, Tribologia-Fin. J. Tribol., 19 (**2000**), 3–18

[15] P. A. Steinmann, Y. Tardy, H. E. Hintermann, Adhesion testing by the scratch test method: the influence of intrinsic and extrinsic parameters on the critical load, Thin Solid Films, 154 (**1987**), 333–349

[16] P. J. Burnett, D. S. Rickerby, The relationship between hardness and scratch adhesion, Thin Solid Films, 154 (**1987**), 403–416

[17] S. J. Bull, Failure modes in scratch adhesion testing, Surf. Coat. Technol., 50 (**1991**), 25–32

[18] S. J. Bull, Spallation failure maps from scratch testing, Mater. High Temp., 13 (**1995**), 169–174

[19] S. J. Bull, Failure mode maps in the thin film scratch adhesion test, Tribol. Int., 30 (**1997**), 491–498

[20] S. T. Gonczy, N. Randall, An ASTM standard for quantitative scratch adhesion testing of thin, hard ceramic coatings, Int. J. Appl. Ceram. Tech., 2 (**2005**), 422–428

[21] W. C. Oliver, G. M. Pharr, An improved technique for determining hardness and elastic-modulus using load and displacement sensing indentation experiments, J. Mater. Res., 7 (**1992**), 1564–1583

[22] A. E. Giannakopoulos, S. Suresh, Determination of elastoplastic properties by instrumented sharp indentation, Scripta Mater., 40 (**1999**), 1191–1198

[23] A. E. Giannakopoulos, P. L. Larsson, R. Vestergaard, Analysis of vickers indentation, Int. J. Solids Struct., 31 (**1994**), 2679–2708

[24] Y. F. Gao, H. T. Xu, W. C. Oliver, G. M. Pharr, Effective elastic modulus of film-on-substrate systems under normal and tangential contact, J. Mech. Phys. Solids, 56 (**2008**), 402–416

[25] S. Shim, H. Bei, E. P. George, G. M. Pharr, A different type of indentation size effect, Scripta Materialia, 59 (**2008**), 1095–1098

[26] Y. Huang, F. Zhang, K. C. Hwang, W. D. Nix, G. M. Pharr, G. Feng, A model of size effects in nano-indentation, J. Mech. Phys. Solids, 54 (**2006**), 1668–1686

[27] G. M. Pharr, Measurement of mechanical properties by ultra-low load indentation, Mat. Sci. Eng. A- Struct., 253 (**1998**), 151–159

[28] Y. Gogotsi, T. Miletich, M. Gardner, M. Rosenborg, Microindentation device for in situ study of pressure-induced phase transformations, Rev. Sci. Instrum., 70 (**1999**), 4612–4617

[29] W. Zhu, P. J. M. Bartos, Application of depth-sensing microindentation testing to study of interfacial transition zone in reinforced concrete, Cement Concrete Res., 30 (**2000**), 1299–1304

[30] O. Uzun, U. Kolemen, S. Celebi, N. Guclu, Modulus and hardness evaluation of polycrystalline superconductors by dynamic microindentation technique, J. Eur. Ceram. Soc., 25 (**2005**), 969–977

[31] Z. Shan, S. K. Sitaraman, Elastic–plastic characterization of thin films using nanoindentation technique, Thin Solid films, 437 (**2003**), 176–181

[32] A. E. Giannakopoulos, S. Suresh, Scr. Mater., 40 (**1999**), 1191

[33] R. P. Vinci, J. J. Vlassak, Annu. Rev. Mater. Sci., 26 (**1996**), 431

[34] W. D. Nix, Mater. Sci. Eng. A, 237 (**1997**), 37

[35] L. De Fazio, S. Syngellakis, R. J. K. Wood, F. M. Fugiule, G. Sciume, Nanoindentation of CVD diamond: comparison of an FE model with analytical and experimental data, Diam. Relat. Mater., 10 (**2001**), 765–769

[36] J. Lia, W. Beres, Three-dimensional finite element modelling of the scratch test for a TiN coated titanium alloy substrate, Wear, 260 (**2006**), 1232–1242

[37] F. Sandiumenge, T. Puig, J. Rabier, J. Plain, X. Obradors, Optimization of flux pinning in bulk melt textured 1–2–3 superconductors; Bringing dislocations under control, Adv. Mater., 12 (**2000**), 375

[38] S. Block, G. J. Piermarini, R. G. Munro, W. Wong-Ng, The bulk modulus and Young's modulus of the superconductor Ba$_2$Cu$_3$YO$_7$, Adv. Ceram. Mater., 2 (**1987**), 601

[39] H. T. Johansen, Flux-pinning-induced stress and magnetostriction in bulk superconductors, Superconducting Science and Technology, 13 (**2000**), 121–137

[40] H. M. Ledbetter, M. W. Austin, S. A. Kim, M. Lei, Elastic constants and Debye temperature of polycrystalline yttrium barium copper oxide (YBa$_2$Cu$_3$O$_{7-x}$), J. Mater. Res., 2 (**1987**), 786

[41] J. J. Roa, X. G. Capdevila, M. Martinez, F. Espiell, M. Segarra, Nanohardness and Young's modulus of YBCO samples textured by the Bridgman technique, Nanotechnology, 18 (**2007**), 385